Hierarchically Self-Assembled Block Copolymer Blends for Templating Hollow Phase-change Nanostructures with an Extremely Low Switching Current

Woon Ik Park^{1,2}, Jong Min Kim¹, Jae Won Jeong¹, Yoon Hyoung Hur¹, Young Joong Choi⁵, Se-Hun Kwon⁵, Seungbum Hong³, You Yin^{4*}, Yeon Sik Jung^{1*} and, Kwang Ho Kim^{2,5*}

¹Department of Materials Science and Engineering, Korea Advanced Institute of Science and Technology (KAIST), 291 Daehak-ro, Yuseong-gu, Daejeon 305-701, Republic of Korea

²Global Frontier R&D Center for Hybrid Interface Materials (HIM), Busandaehak-ro 63beon-gil, Geumjeong-gu, Busan 609-735, Republic of Korea

³Materials Science Division, Argonne National Laboratory, Lemont, IL 60439, USA

⁴Graduate School of Engineering, Gunma University, 1-5-1 Tenjin, Kiryu, Gunma 376-8515, Japan

⁵School of Materials Science and Engineering, Pusan National University, Busandaehak-ro 63beon-gil, Geumjeonggu, Busan 609-735, Republic of Korea

KEYWORDS: block copolymers, blend, self-assembly, phase change memory, non-volatile memory

ABSTRACT: Phase change memory (PCM) is one of the most promising candidates for next-generation non-volatile memory devices due to its high speed, excellent reliability, and outstanding scalability. However, the high switching current of PCM devices has been a critical hurdle to realize low-power operation. Although one solution is to reduce the switching volume of the memory, the resolution limit of photolithography hinders further miniaturization of device dimensions. In this study, we employed unconventional self-assembly geometries obtained from blends of block copolymers (BCPs) to form ring-shaped hollow PCM nanostructures with an ultra-small contact area between a phase-change material ($Ge_2Sb_2Te_5$) and a heater (TiN) electrode. The high-density (approximately 0.1 terabits per square inch) PCM nanoring arrays showed extremely small switching current of 2 – 3 μ A. Furthermore, the relatively small reset current of the ring-shaped PCM compared to the pillar-shaped devices is attributed to smaller switching volume, which is well supported by electro-thermal simulation results. This approach may also be extended to other non-volatile memory device applications such as resistive switching memory and magnetic storage devices, where the control of nanoscale geometry can significantly

INTRODUCTION

As one of the viable candidates of the next-generation non-volatile memories, phase change memory (PCM) has attracted considerable attention due to its rapid cell operation, excellent reliability, and good scalability.1-7 PCM, which exploits the phase transition phenomenon of a chacogenide material, has roughly two orders of difference in electrical resistance between the crystalline and amorphous states.4 Most chacogenide materials (e.g. Ge₂Sb₂Te₅, GST) have a high melting temperature (~ 888K), requiring high reset current to operate the PCM cells.^{4,8} For this reason, considerable research efforts have been devoted to developing new phase-change materials, designing novel device structures, and improving interfaces for lower power consumption, higher density, and better scalability. 4, 9-18 For portable device applications in particular, a PCM device structure with a higher integration density and a small contact area is required for device operation with low-power consumption. 10, 17-19 Although the reset current scales down with the contact area between the phase change material and the heater material, a practical fabrication route for high-density PCM cell arrays with dramatically enhanced performance has not been achieved, partially because of the resolution limit of photolithography and the increased cost for advanced nanolithography technologies. 10 Therefore, more practical approaches to simultaneously address the two challenges of higher integration density and smaller reset current should be developed.

In this study, we report a facile route to fabricate nanoring-shaped PCM cell arrays with a small contact area between Ge₂Sb₂Te₅ (GST) and TiN using the nanoscale morphology formed by self-assembly of block copolymer (BCP) blends to achieve low-power operation of PCM. First, we used the hierarchical self-assembly of BCP

blends, which can generate dot-in-hole nanostructures diblock from two different **BCPs** poly(dimethylsiloxane-b-styrene) (PDMS-b-PS) and poly(styrene-*b*-ferrocenyldimethylsilane) (PS-b-PFS) (Figure 1a) after plasma oxidation. The self-assembled morphology from the two Si-containing BCPs can easily be converted into oxide nanostructures after a short reactive ion etch (RIE) with an O2 plasma, and the oxide nanostructure can serve as a useful nanotemplate for fabricating ring-shaped phase-change nanostructures (Figure 1b). Second, we also report extremely low power operation from ring-shaped PCM memory devices with a small contact area. The current-voltage characteristics of the ultra-small ring-shaped PCM cells were measured by conductive atomic force microscopy (C-AFM) using a Ptcoated tip. Furthermore, the simulation results theoretically support that smaller reset current can be achieved with the ring-shaped PCM cell arrays compared to pillarshaped PCM devices.

EXPERIMENTAL SECTION

PCM device fabrication. After W (200 nm, bottom electrode) was sputter-deposited on a SiO_2 (200 nm)/Si substrate, heater TiN (50 nm) and the phase-change material $Ge_2Sb_2Te_5$ (GST) (30 nm) were formed sequentially on the substrate. In order to stabilize the self-assembly of BCP, the surface of the GST thin film was treated with a hydroxy-terminated PS homopolymer with a molecular weight (MW) of 41 kg/mol, which was vacuum annealed at 150 oC for 2 hours and washed with toluene. After surface fuctionalization of the GST film, hole-in-dot nanostructures were made by host-guest self-assembly of block copolymers. Pt was sputter-deposited on the sample followed by CF_4 plasma etching at 200W for 4 minutes. After formation of the Pt nano-ring, GST nanorings were patterned using the structures as etch masks.

Host-guest self-assembly of block copolymer. All of the BCPs (DS45 and SF35) with a minority block volume fraction $(f_{PDMS}^{dry}) = 33.7\%$ and $(f_{PDMS}^{dry}) = 11.5\%$ were purchased from Polymer Source, Inc. The BCPs dissolved in toluene were mixed at a volume ratio of 2.5 to 1, and then spin-coated on the substrate. The microphase-separated dot-in-hole (guest-host) nanostructure was obtained by solvent annealing in the binary solvents of heptane and toleuen ($V_{HEP}/V_{TOL} = 1.2$) at 85 °C for 30 minutes. To generate the binary solvent vapor, we used a stainless chamber (full capacity = 40 mL) with binary solvents (15 mL) of heptane and toluene. The annealed sample was etched by CF₄ plasma (time = 20 sec, working pressure = 15 mTorr, and plasma source power = 6oW) followed by O₂ plasma (30 sec, 15mT, and 5oW) to obtain the desired dot (ox-PFS, guest) in hole (ox-PDMS, host) nanostructures using reactive ion etching (RIE). All SEM, AFM, and TEM images were taken after the two-step plasma etching step.

RESULTS AND DISCUSSION

Figure 1 shows a schematic illustration of host-guest self-assembly of BCP blends and the ring-shaped PCM

nanostructure obtained through a pattern-reversal process. BCP self-assembly is driven by the spontaneous microphase-separation of two or more mutually incompatible blocks, and is one of the most practical candidates to generate and tune high-density functional nanostructures. 20-24 The combination of BCP self-assembly and photolithography has garnered wide attention as a useful fabrication route due to its excellent pattern resolution, scalability, and compatibility with conventional semiconductor processes.^{25, 26} It can produce sub-20 nm pattern arrays with several geometries such as lines, dots, and holes; furthermore, the self-assembled nanoscale patterns can readily be transferred onto diverse functional materials including oxides, metals, and organic materials.27-41 However, in general, pure diblock BCPs present limited types of morphologies.33

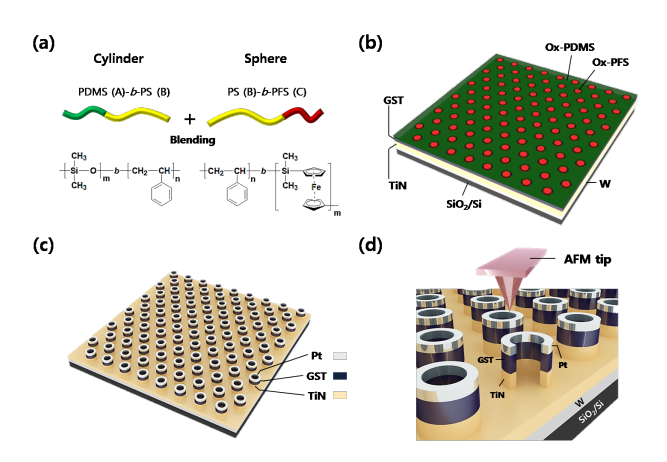


Figure 1. Schematic of methodology of self-assembled BCP nanostructure using BCP blends, and pattern-reversed PCM ring arrays. (a) BCP blends of cylinder-forming PDMS-*b*-PS (DS45) and sphere-forming PS-*b*-PFS (SF35), (b) Self-assembled nanostructure formed by using BCP blends of DS45 and SF35, (c) Ring-shaped PCM cell arrays formed by pattern reversal process, (d) Magnified ring-shaped PCM devices under C-AFM measurement.

As we previously reported in detail, 42 apart from using pure diblock BCPs, uniformly microphase-separated morphologies also can be obtained from a mixture of A-b-B and B-b-C BCPs by precisely controlling the mixing ratio of two BCPs and the volume ratio of binary solvents (heptane and toluene). We employed PDMS-b-PS (DS45) with a molecular weight (MW) of 45.5 kg/mol and PS-b-PFS (SF35) with a MW of 35 kg/mol. It was demonstrated that the effective volume fraction of PDMS can be controlled by changing the volume fraction of heptane in the mixture solvent used for solvent vapor annealing. At the optimum mixing ratios of the two BCPs and mixture solvents, a hexagonally perforated lamellar (HPL) microdomain (DS45, host) accommodating spherical structures (SF35, guest) can be formed on a GST/TiN/W/SiO3/Si substrate via the hierarchical self-assembly of A-b-B/B-b-C BCP blends (Figures 1a-1b). The self-assembled dot-inhole nanostructure was used as a template to produce ring-shaped PCM nanostructures. Their electrical properties were measured by C-AFM, as schematically described in Figures 1c-1d.

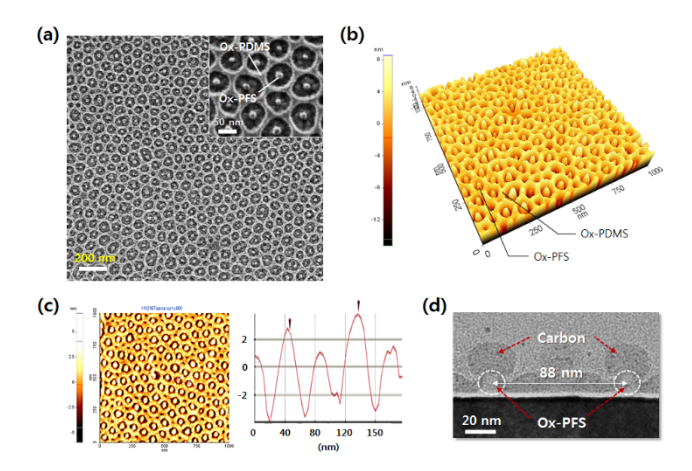


Figure 2. Oxide nanostructures derived from BCP blends. (a) SEM image of dots (oxidized PFS: $SiFe_yO_z$) in holes (oxidized PDMS: SiO_x) nanostructure. (b) 3D topographic AFM image of (a). (c) AFM line-scan profile of the oxide nanostructures. Center-to-center distance of ~ 88 nm was measured from the AFM data. (d) Cross-sectional TEM image for the dot-to-dot distance.

Figure 2a shows that a one-to-one matched nanostructure *via* host-guest self-assembly was successfully formed over the GST thin film. Each oxidized PFS (ox-PFS) nanodot with a diameter of 20 nm was positioned at the center of the 65-nm-sized hole in oxidized PDMS (ox-PDMS). The three-dimensional AFM image in Figure 2b shows the well-defined self-assembly morphology of the binary BCP blend after RIE treatment. We also obtained and analyzed top-view AFM and cross-sectional transmission electron microscopy (TEM) images, as presented in Figures 2c-2d. The line profile of the AFM and TEM images confirms that the average center-to-center distance of the ox-PFS nanodots is about 88 nm.

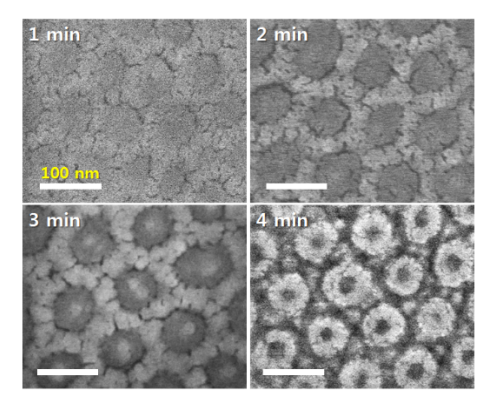


Figure 3. Pattern-transferred PCM nanostructures. Ringshaped PCM cell arrays formed by pattern reversal process as a function of the etching time of CF₄ plasma after Pt deposition.

After Pt was sputter-deposited on the dot-in-hole oxide nanostructure, the sample was back-etched using ${\rm CF_4}$

plasma, showing a reverse Pt nano-ring pattern in 4 minutes. Figure 4 shows the Pt nano-ring structures obtained by the pattern transfer process as a function of the etch time of CF_4 plasma. The Pt nano-ring arrays can be utilized as hard masks for patterning GST/TiN/W as well as top electrodes because the Pt nano-ring is more etch resistant under CF_4 plasma than GST and TiN.

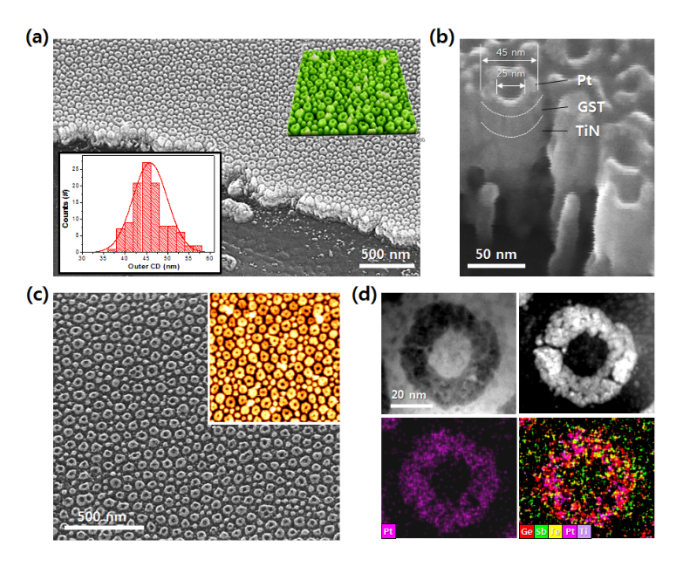


Figure 4. Ring-shaped PCM nanostructures formed using dot-in-hole nanostructure as a template. (a) Tilted SEM image of the ring-shaped PCMs. The inset is a topographic AFM image of the ring-shaped PCM devices. Inset: Outer CD distribution of PCM cell arrays, (b) Magnified SEM image of the ring-shaped PCM cells with an outer and inner CD of 45 nm and 25 nm, respectively. (c) PCM arrays formed over a large area. Inset: topographic AFM top-view image, (d) Top-view TEM images: bright field (top, left) and dark-field (top, right), and EDS elemental mapping images of Pt (bottom, left) and total (bottom, right).

We demonstrate the formation of uniformly formed high-density ring-shaped PCM cell arrays over a large area. The ring-shaped PCM cell arrays were prepared using a Pt nano-ring as an etch mask, which has a very high density (~ 0.1 terabits per square inches), without using high-cost lithography techniques (Figures 4a, 4b, and 4c). The insets of Figure 4a show the tilted AFM image of PCM structures (right) and statistical distribution of the outer critical dimension (CD) of the ring-shaped PCM arrays (left). For a PCM device, the contact area of GST and TiN plays a key role to reduce power consumption because the reset current of PCM decreases in proportion with the contact area. The ring-shaped PCM device with outer and inner diameters of 45 nm and 25 nm has a very small contact area (~ 491 nm²) between the heater and the GST layer due to its hollow structure. The formation of a hollow PCM device via the self-assembly of BCP blends was confirmed by the TEM analysis results shown in Figure 4d. The energy-dispersive X-ray spectroscopy (EDS) elemental mapping of Pt (Figure 4d, left-bottom), and Ge, Sb, Te, Ti, and Pt (Figure 4d, right-bottom) also suggests that the PCM cells have a hollow ring-shaped structure. Additional TEM analysis and elemental mapping results are provided in Figure S1.

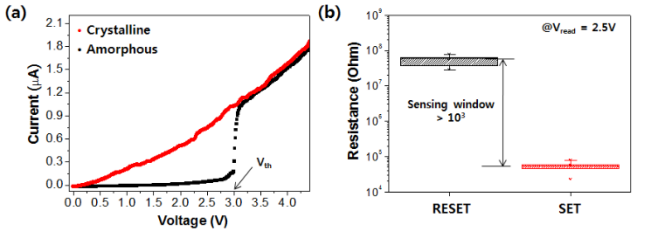


Figure 5. Electrical property of ring-shaped PCM arrays. (a) I-V scan curve of a PCM device. (b) Distributions of RESET and SET resistance at a read voltage of 2.5V.

To investigate the electrical characteristics of the ring-shaped Pt/GST/TiN/W PCM device, we used a C-AFM with a tip radius of 30 nm. For measurement of the current-voltage (I-V) characteristics, a bias voltage was swept over Pt (top electrode, TE) from o to 5 V with a step size of o.o₁V, while the W (bottom electrode, BE) was grounded. The results show a typical phase-change behavior with a transition from the high resistance (amorphous) to the low resistance (crystalline) state. Its threshold voltage was about 3.0 V, showing more than two orders of difference in resistance (sensing window > 103) at a read voltage of 2.5 V (Figures 5a-5b). Figure 5b shows the resistance distribution of SET (crystalline) and RESET (amorphous) states. The reset current to switch from the amorphous to crystalline state was approximately 2 µA, which is a very low value compared to previous reports. It should be emphasized that the measured reset current of the ring-shaped PCM cells is comparable with the lowest switching current reported to date. 43 We attribute the low switching current to the small switching volume of the nanostructure resulting from the structural hollowness of the PCM structure.

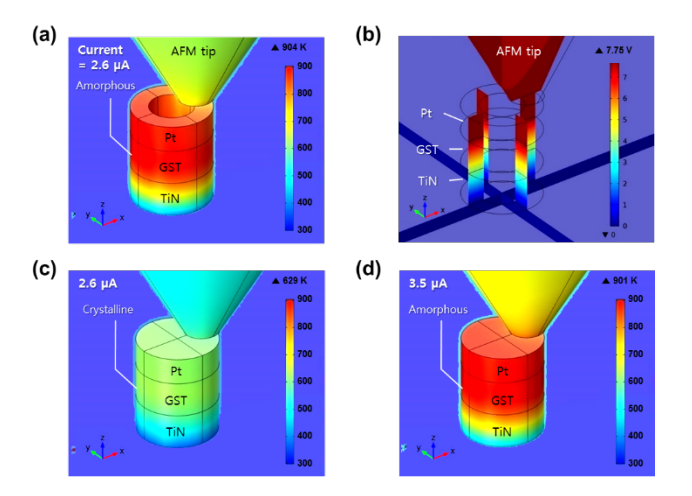


Figure 6. Electro-thermal simulations for the ring and pillar PCM devices. (a, c, d) Temperature distributions of (a) a ring-shaped PCM device and (c & d) a pillar-shaped PCM device, (b) Electric potential distribution of (b) a ring-shaped PCM device. The applied current pulses were (a) 2.6 μ A, (c) 2.6 μ A, and (d) 3.5 μ A, respectively. The ring-shaped PCM device has lower switching current than the pillar-

shaped PCM device. While the pillar-shaped PCM device was not switched when the current of 2.6 μ A is applied, a pulsed current of 3.5 μ A enabled the reset operation by reaching the melting point of GST.

Furthermore, we theoretically calculated the performance of the ring-shaped PCM device using the electrothermal method. In order to explore the effects of the structural hollowness, two PCM structures with and without a central hole were compared. We calculated the temperature and electric potential distributions in the GST based on the reset current (~ 2 µA) obtained from C-AFM measurement. When a reset pulse of 2.6 µA was applied with a duration time of 150 ns to the ring-shaped PCM device, the maximum temperature (T_{max}) in the memory nanostructure was calculated to be 904K, as shown in Figures 6a-6b. The temperature is above the melting point (T_{melt}, 888K) of GST, suggesting the formation of fully amorphized GST after quenching (RESRT operation). In contrast, when the same reset pulse of current was applied to the pillar-shaped PCM device, the T_{max} of the GST was calculated to be only 629K (Figure 6c), which is sufficiently lower than T_{melt}. On the other hand, when the higher reset current pulse of 3.5 µA was applied to the device, the temperature of GST rose slightly above T_{melt}, as shown in Figure 6d. These simulation results indicate that for the pillar-shaped PCM device with a larger contact area (1,590 nm²) between GST and TiN, 134% higher reset current was required to switch the PCM cell compared to the hollow ring-shaped PCM (contact area = 491 nm²). We also anticipate that PCM ring arrays with smaller dimensions may be obtained by controlling the self-assembly conditions such as the use of BCPs with smaller MWs, leading to additional power reduction and higher device integration density.

CONCLUSION

In summary, we introduced a unique ring-shaped PCM cell array structure with small contact area between $Ge_2Sb_2Te_5$ (GST) and heater TiN using a complex self-assembled nanostructure from BCP blends. The ultrahigh-density PCM ring arrays showed extremely small switching current of 2 – 3 μ A. Simulation results support that ultra-small reset current of ring-shaped PCM can be obtained compared to pillar-shaped PCM devices, resulting from the hollow nature of the structure. The nanoring geometry may also be extended to other memory device applications such as resistive switching memory and magnetic memory elements, where device performances can be significantly affected by the subtle control of nanoscale geometries.

ASSOCIATED CONTENT

Supporting Information. TEM-EDS data for ring-shaped PCM device and experimental methods. This material is available free of charge via the Internet at http://pubs.acs.org.

AUTHOR INFORMATION

Corresponding Author

*Email: kwhokim@pusan.ac.kr (K.H.K.), ysjung@kaist.ac.kr (Y.S.J.), yinyou@gunma-u.ac.jp (Y.Y)

Author Contributions

K.H.K, Y.S.J, and W.I.P. conceived and designed the experiments. W.I.P., J.M.K., J.W.J., Y.H.H., and Y.J.C. performed the experiments (self-assembly, SEM, AFM, TEM analyses). Y.Y performed PCM simulations. W.I.P and Y.S.J wrote the majority of the manuscript. All authors discussed the results and commented on the manuscript at all stages.

Notes

The authors declare no competing financial interest.

ACKNOWLEDGMENT

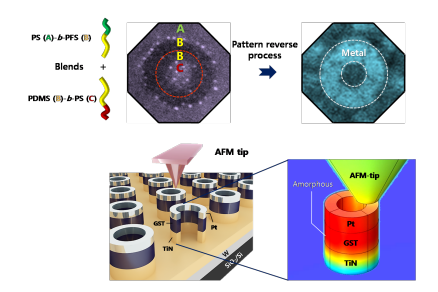
This research was mainly supported by Global Frontier Program through the Global Frontier Hybrid Interface Materials (GFHIM) of the National Research Foundation of Korea (NRF) funded by the Ministry of Science, ICT & Future Planning (2013M3A6B1078874). The work at Argonne (S.H., data analysis and manuscript writing) was supported by U.S. Department of Energy, Office of Basic Energy Sciences, Materials Sciences and Engineering Division.

REFERENCES

- (1) Derbyshire, K., Solid State Technol 2011, 54, 7.
- (2) Wuttig, M.; Yamada, N., Nat. Mater. 2007, 6, 824-832.
- (3) Hamann, H. F.; O'Boyle, M.; Martin, Y. C.; Rooks, M.; Wickramasinghe, K., Nat. Mater. 2006, 5, 383-387.
- (4) Wong, H. S. P.; Raoux, S.; Kim, S.; Liang, J. L.; Reifenberg, J. P.; Rajendran, B.; Asheghi, M.; Goodson, K. E., *P. IEEE* **2010**, *98*, 2201-2227.
- (5) Raoux, S.; Burr, G. W.; Breitwisch, M. J.; Rettner, C. T.; Chen, Y. C.; Shelby, R. M.; Salinga, M.; Krebs, D.; Chen, S. H.; Lung, H. L.; Lam, C. H., *IBM J. Res. Dev.* **2008**, 52, 465-479.
- (6) Lencer, D.; Salinga, M.; Wuttig, M., Adv. Mater. 2011, 23, 2030-2058.
- (7) Hong, S.; Auciello, O.; Wouters, D. *Emerging Non-Volatile Memories*; Springer: **2014**; Chapter 4.
- (8) Kolobov, A. V.; Fons, P.; Krbal, M.; Simpson, R. E.; Hosokawa, S.; Uruga, T.; Tanida, H.; Tominaga, J., *Appl. Phys. Lett.* **2009**, *95*, 1902.
- (9) Jeong, C. W.; Ahn, S. J.; Hwang, Y. N.; Song, Y. J.; Oh, J. H.; Lee, S. Y.; Lee, S. H.; Ryoo, K. C.; Park, J. H.; Park, J. H.; Shin, J. M.; Yeung, F.; Jeong, W. C.; Kim, J. I.; Koh, G. H.; Jeong, G. T.; Jeong, H. S.; Kim, K., *Jpn. J. Appl. Phys.* **2006**, *45*, 3233-3237.
- (10) Lacaita, A. L., Solid State Electron 2006, 50, 24-31.
- (11) Kim, C.; Suh, D. S.; Kim, K. H. P.; Kang, Y. S.; Lee, T. Y.; Khang, Y.; Cahill, D. G., *Appl. Phys. Lett.* **2008**, *92*.
- (12) Kao, K. F.; Lee, C. M.; Chen, M. J.; Tsai, M. J.; Chin, T. S., *Adv. Mater.* **2009**, *21*, 1695-1699.
- (13) Simpson, R. E.; Fons, P.; Kolobov, A. V.; Fukaya, T.; Krbal, M.; Yagi, T.; Tominaga, J., *Nat. nanotechnol.* **201**, *6*, 501-505.
- (14) Yao, D. N.; Zhou, X. L.; Wu, L. C.; Song, Z. T.; Cheng, L. M.; Rao, F.; Liu, B.; Feng, S. L., *Solid State Electron* **2013**, *79*, 138-141.
- (15) Lee, S. H.; Jung, Y.; Agarwal, R., *Nat. nanotechnol.* **2007**, 2, 626-630.
- (16) Park, W. I.; You, B. K.; Mun, B. H.; Seo, H. K.; Lee, J. Y.; Hosaka, S.; Yin, Y.; Ross, C. A.; Lee, K. J.; Jung, Y. S., *ACS Nano* **2013**, 7, 2651-2658.

- (17) Lencer, D.; Salinga, M.; Wuttig, M., Adv. Mater. 2011, 23, 2030-2058.
- (18) A. Pirovano, A. L. L., A. Benvenuti, F. Pellizzer, S. Hudgens, and R. Bez. *IEDM* **2003**, 29.6.1-29.6.4.
- (19) Ryoo, K. C.; Song, Y. J.; Shin, J. M.; Park, S. S.; Lim, D. W.; Kim, J. H.; Park, W. I.; Sim, K. R.; Jeong, J. H.; Kang, D. H.; Kong, J. H.; Jeong, C. W.; Oh, J. H.; Park, J. H.; Kim, J. I.; Oh, Y. T.; Kim, J. S.; Eun, S. H.; Lee, K. W.; Koh, S. P.; Fai, Y.; Koh, G. H.; Jeong, G. T.; Jeong, H. S.; Kim, K., *Jpn. J. Appl. Phys.* **2007**, *46*, 2001-2005.
- (20) Thurn-Albrecht, T.; Schotter, J.; Kastle, C. A.; Emley, N.; Shibauchi, T.; Krusin-Elbaum, L.; Guarini, K.; Black, C. T.; Tuominen, M. T.; Russell, T. P., *Science* **2000**, 290, 2126-2129.
- (21) Park, W. I.; Yoon, J. M.; Park, M.; Lee, J.; Kim, S. K.; Jeong, J. W.; Kim, K.; Jeong, H. Y.; Jeon, S.; No, K. S.; Lee, J. Y.; Jung, Y. S., *Nano Lett.* **2012**, *12*, 1235-1240.
- (22) Jung, Y. S.; Jung, W.; Ross, C. A., Nano Lett. 2008, 8, 2975-2981.
- (23) Chai, J.; Wang, D.; Fan, X. N.; Buriak, J. M., Nat. nanotechnol. 2007, 2, 500-506.
- (24) Zhang, X. J.; Qiao, Y. H.; Xu, L. N.; Buriak, L. M., ACS Nano 2011, 5, 5015-5024.
- (25) Jung, Y. S.; Chang, J. B.; Verploegen, E.; Berggren, K. K.; Ross, C. A., *Nano Lett.* **2010**, *10*, 1000-1005.
- (26) Jeong, J. W.; Park, W. I.; Do, L. M.; Park, J. H.; Kim, T. H.; Chae, G.; Jung, Y. S., *Adv. Mater.* 2012, 24, 3526-3531.
- (27) Park, M.; Harrison, C.; Chaikin, P. M.; Register, R. A.; Adamson, D. H., *Science* 1997, 276, 1401-1404.
- (28) Segalman, R. A.; Yokoyama, H.; Kramer, E. J., *Adv. Mater.* **2001**, *13*, 1152-1155.
- (29) Kim, S. O.; Solak, H. H.; Stoykovich, M. P.; Ferrier, N. J.; de Pablo, J. J.; Nealey, P. F., *Nature* **2003**, *424*, 411-414.
- (30) Cheng, J. Y.; Mayes, A. M.; Ross, C. A., *Nat. Mater.* **2004**, 3, 823-828.
- (31) Stoykovich, M. P.; Muller, M.; Kim, S. O.; Solak, H. H.; Edwards, E. W.; de Pablo, J. J.; Nealey, P. F., *Science* **2005**, 308, 1442-1446
- (32) Segalman, R. A., Mat Sci Eng R 2005, 48, 191-226.
- (33) Black, C. T.; Ruiz, R.; Breyta, G.; Cheng, J. Y.; Colburn, M. E.; Guarini, K. W.; Kim, H. C.; Zhang, Y., *IBM J. Res. Dev.* **2007**, *51*, 605-633.
- (34) Darling, S. B., Prog Polym Sci 2007, 32, 1152-1204.
- (35) Bita, I.; Yang, J. K. W.; Jung, Y. S.; Ross, C. A.; Thomas, E. L.; Berggren, K. K., *Science* **2008**, 321, 939-943.
- (36) Ruiz, R.; Kang, H. M.; Detcheverry, F. A.; Dobisz, E.; Kercher, D. S.; Albrecht, T. R.; de Pablo, J. J.; Nealey, P. F., *Science* **2008**, 321, 936-939.
- (37) Jung, Y. S.; Jung, W.; Tuller, H. L.; Ross, C. A., *Nano Lett.* **2008**, *8*, 3776-3780.
- (38) Jung, Y. S.; Ross, C. A., Adv. Mater. 2009, 21, 2540-2545.
- (39) Lee, J.; Kim, K.; Park, W. I.; Kim, B. H.; Park, J. H.; Kim, T. H.; Bong, S.; Kim, C. H.; Chae, G.; Jun, M.; Hwang, Y.; Jung, Y. S.; Jeon, S., *Nano Lett.* **2012**, *12*, 6078-6083.
- (40) Tavakkoli, K. G. A.; Gotrik, K. W.; Hannon, A. F.; Alexander-Katz, A.; Ross, C. A.; Berggren, K. K., *Science* **2012**, *336*, 1294-1298.
- (41) Jeong, J. W.; Yang, S. R.; Hur, Y. H.; Kim, S. W.; Baek, K. M.; Yim, S.; Jang, H. I.; Park, J. H.; Lee, S. Y.; Park, C. O.; Jung, Y. S., *Nat. Comm.* **2014**, *5*, *5*387.
- (42) Park, W. I.; Kim, Y.; Jeong, J. W.; Kim, K.; Yoo, J. K.; Hur, Y. H.; Kim, J. M.; Thomas, E. L.; Alexander-Katz, A.; Jung, Y. S., *Scientific reports* **2013**, *3*, 3190.
- (43) Xiong, F.; Liao, A. D.; Estrada, D.; Pop, E., *Science* **2011**, 332, 568-570.

Table of Contents graphic and summary



Summary: Ring-shaped PCM cells with small contact area between $Ge_2Sb_2Te_5$ and TiN using a self-assembled nanostructure from BCP blends showed extremely small switching current of 2–3 μ A. Simulations support that ultra-small reset current of ring-shaped PCM can be obtained compared to pillar-shaped PCM, resulting from the hollow nature of the structure.